

Identifying non-Hermitian critical points with quantum metric

Jun-Feng Ren,^{1,2} Jing Li,^{1,2} Hai-Tao Ding,^{3,4,5,*} and Dan-Wei Zhang^{1,2,†}

¹*Key Laboratory of Atomic and Subatomic Structure and Quantum Control (Ministry of Education), Guangdong Basic Research Center of Excellence for Structure and Fundamental Interactions of Matter, South China Normal University, Guangzhou 510006, China*

²*Guangdong Provincial Key Laboratory of Quantum Engineering and Quantum Materials, School of Physics, South China Normal University, Guangzhou 510006, China*

³*National Laboratory of Solid State Microstructures and School of Physics, Nanjing University, Nanjing 210093, China*

⁴*Collaborative Innovation Center of Advanced Microstructures, Nanjing 210093, China*

⁵*Department of Physics, National University of Singapore, Singapore 117551*

(Dated: May 2, 2024)

The geometric properties of quantum states is fully encoded by the quantum geometric tensor. The real and imaginary parts of the quantum geometric tensor are the quantum metric and Berry curvature, which characterize the distance and phase difference between two nearby quantum states in Hilbert space, respectively. For conventional Hermitian quantum systems, the quantum metric corresponds to the fidelity susceptibility and has already been used to specify quantum phase transitions from the geometric perspective. In this work, we extend this wisdom to the non-Hermitian systems for revealing non-Hermitian critical points. To be concrete, by employing numerical exact diagonalization and analytical methods, we calculate the quantum metric and corresponding order parameters in various non-Hermitian models, which include two non-Hermitian generalized Aubry-André models and non-Hermitian cluster and mixed-field Ising models. We demonstrate that the quantum metric of eigenstates in these non-Hermitian models exactly identifies the localization transitions, mobility edges, and many-body quantum phase transitions, respectively. We further show that this strategy is robust against the finite-size effect and different boundary conditions.

I. INTRODUCTION

Quantum phase transitions are a kind of phase transitions that are driven by quantum fluctuations and occur at zero temperature [1]. They are extensively investigated between different magnetic phases [2], localization phases [3–6], topological phases [7–10], and so on. Near the phase transition point, the infinitesimal variation of certain system parameters will dramatically change the properties of the ground (eigen) state, which intuitively leads to a sharp change of the state fidelity. Moreover, an information-geometric approach based on this observation has already been put forward [11–18]. The concrete procedure is to calculate the fidelity susceptibility, which defines the response of fidelity to the driving parameter of the system Hamiltonian near critical points [11–16].

The fidelity susceptibility is closely related to the quantum metric, which characterizes the distance between two nearby quantum states in Hilbert space [19–22]. The quantum metric is the real part of a more general geometric concept, called the quantum geometric tensor (QGT) [19, 23], of which the imaginary part is the well-studied Berry curvature [24–26] for plenty of celebrated physical effects [27–33]. The quantum metric is also related to many fascinating physical phenomena, such as the superfluidity in flat bands [34, 35] and topological quantum phases [36–38]. The quantum metric has recently been experimentally measured in various artificial

quantum systems [39–52].

Most of these previous studies focus on the QGT and related quantum phase transitions in Hermitian systems [53–61]. In recent years, the theoretical and experimental explorations of non-Hermitian physics have garnered significant attentions [62–85]. Various novel phenomena or phases unique to non-Hermitian systems have been revealed, such as exceptional points [72–74, 86–89], non-Hermitian skin effects [75–77], and non-Hermitian delocalization [78–83]. It is worth mentioning that phase transitions could be also sensitive to the non-Hermiticity, and the associated critical points in non-Hermitian systems have potential for sensitivity enhancement in the quantum sensing regime [84, 85, 90–92].

Here we exploit the information-geometric approach to study quantum phase transitions in both single-particle and many-body non-Hermitian systems. We explore the critical points in various non-Hermitian models through the quantum metric. By using the numerical exact diagonalization, we calculate the quantum metric and localization properties (the fractal dimension and participation ratio) in two non-Hermitian generalized Aubry-André (GAA) models [93–95]. Our results show that the quantum metric will be divergent or singular in proximity of localization transition points for all eigenstates. Thus the quantum metric exactly identifies the localization transition and the mobility edges in these non-Hermitian quasiperiodic systems. For non-Hermitian cluster and mixed-field Ising models, we demonstrate that the quantum metric of the ground state can reveal the quantum phase transitions, as compared with the corresponding order parameters obtained from both an-

* ht ding@smail.nju.edu.cn

† danweizhang@m.scnu.edu.cn

alytical and numerical approaches. Finally, we show that this information-geometric strategy for identifying non-Hermitian critical points is robust against the finite-size effect and different boundary conditions.

The rest of this paper is organized as follows. A brief review of the quantum metric for non-Hermitian Hamiltonians is given in Sec. II. In Sec. III, we identify the localization transitions and mobility edges in two non-Hermitian GAA models through the quantum metric of eigenstates, respectively. Sec. IV is devoted to revealing quantum phase transitions in non-Hermitian cluster and mixed-field Ising models with the quantum metric of ground states. Brief discussions on the finite-size effect and boundary conditions and a short conclusion are presented in Sec. V.

II. NON-HERMITIAN QUANTUM METRIC

We begin by considering a non-Hermitian Hamiltonian $H(\boldsymbol{\lambda})$ parameterized by $\boldsymbol{\lambda} = (\lambda_1, \lambda_2, \dots, \lambda_D)$ in D -dimensional parameter space. The eigenstate equation is $H(\boldsymbol{\lambda})|\psi_n^R(\boldsymbol{\lambda})\rangle = E_n|\psi_n^R(\boldsymbol{\lambda})\rangle$ with n the band index. The eigenvalues E_n are in general complex due to the non-Hermiticity of the Hamiltonian, and the eigenstate $|\psi_1^R(\boldsymbol{\lambda})\rangle$ corresponding to the minimum real eigenvalue is set as the ground state. The eigenstates satisfy the normalization condition $\langle\psi_n^R(\boldsymbol{\lambda})|\psi_n^R(\boldsymbol{\lambda})\rangle = 1$ but is generally nonorthogonal $\langle\psi_m^R(\boldsymbol{\lambda})|\psi_n^R(\boldsymbol{\lambda})\rangle \neq 0$ ($m \neq n$). We assume the ground state $|\psi_1^R(\boldsymbol{\lambda})\rangle$ is non-degenerate and focus on the right eigenstates $|\psi_n^R(\boldsymbol{\lambda})\rangle \doteq |\psi_n(\boldsymbol{\lambda})\rangle$ for simplicity. The distance between two neighbor eigenstates $|\psi_n(\boldsymbol{\lambda})\rangle$ and $|\psi_n(\boldsymbol{\lambda} + d\boldsymbol{\lambda})\rangle$ in the parameter space is given by [19, 23, 96]

$$ds^2 = 1 - |\langle\psi_n(\boldsymbol{\lambda})|\psi_n(\boldsymbol{\lambda} + d\boldsymbol{\lambda})\rangle|^2 = \sum_{\mu\nu} g_{\mu\nu}^{(n)} d\lambda_\mu d\lambda_\nu, \quad (1)$$

where $g_{\mu\nu}^{(n)}$ is the non-Hermitian quantum metric with parameters $\{\mu, \nu\} \in (\lambda_1, \lambda_2, \dots, \lambda_D)$. It is the real part of the non-Hermitian quantum geometric tensor [19, 23, 96]

$$\begin{aligned} Q_{\mu\nu}^{(n)} &= \langle\partial_{\lambda_\mu}\psi_n|\partial_{\lambda_\nu}\psi_n\rangle - \langle\partial_{\lambda_\mu}\psi_n|\psi_n\rangle\langle\psi_n|\partial_{\lambda_\nu}\psi_n\rangle \\ &= g_{\mu\nu} - \frac{i}{2}F_{\mu\nu}, \end{aligned} \quad (2)$$

where $g_{\mu\nu}^{(n)} = \text{Re}(Q_{\mu\nu})$, and the imaginary part $F_{\mu\nu} = -2\text{Im}(Q_{\mu\nu})$ corresponds to the Berry curvature.

For identifying the quantum phase transition driven by a single parameter μ , we can consider an infinitesimal change of the parameter: $\mu \rightarrow \mu + d\mu$, and then obtain

$$F_n^2 \doteq |\langle\psi_n(\mu)|\psi_n(\mu + d\mu)\rangle|^2 \approx 1 - \chi_F^{(n)}(d\mu)^2. \quad (3)$$

Here F_n is the so-called fidelity of the n -th eigenstate, and $\chi_F^{(n)}$ is the fidelity susceptibility [11, 14, 18]. Notably, $\chi_F^{(n)}$ denotes the response of F_n due to the small change of μ . Combining Eq. (1) and Eq. (3), we can proof the

equivalence of the quantum metric and the fidelity susceptibility in generic non-Hermitian Hamiltonians [7, 97]:

$$\begin{aligned} g_{\mu\mu}^{(n)} &= \text{Re}(\langle\partial_\mu\psi_n|\partial_\mu\psi_n\rangle - \langle\partial_\mu\psi_n|\psi_n\rangle\langle\psi_n|\partial_\mu\psi_n\rangle) \\ &= \lim_{d\mu \rightarrow 0} \frac{-2 \ln F_n}{d\mu^2} = \chi_F^{(n)}. \end{aligned} \quad (4)$$

It has been shown that the fidelity susceptibility of the ground state can detect quantum critical points in Hermitian systems [11–16]. For n -th eigenstate, one can also expect that the corresponding quantum metric $g_{\mu\mu}^{(n)}$ will reach the maximum value or diverge at its localization transition point. In the following, we extend this wisdom to generic non-Hermitian models. To be concrete, we demonstrate that the localization transition of all eigenstates with related mobility edges and the quantum phase transitions in non-Hermitian disordered and many-body systems can be revealed by the quantum metric, respectively.

III. NON-HERMITIAN LOCALIZATION TRANSITIONS AND MOBILITY EDGES

A. Detecting localization transitions

We first consider a non-Hermitian version of the GAA model with quasi-periodic modulations on both the on-site potential and off-diagonal hopping amplitude [98–100]. Generally, the non-Hermiticities come from the nonreciprocal hopping and complex potential phase, and the model Hamiltonian can be written as [6, 93, 94]

$$H_{\text{GAA}}^{(1)} = \sum_j [t_j(e^{-g}c_{j+1}^\dagger c_j + e^g c_j^\dagger c_{j+1}) + \Delta_j c_j^\dagger c_j], \quad (5)$$

where c_j (c_j^\dagger) is the annihilation (creation) operator at the j -th site. Here g is the dimensionless nonreciprocal strength of the hopping amplitude t_j , and Δ_j is the on-site potential term. They are given by

$$\begin{aligned} t_j &= t + V_2 \cos[2\pi\beta(j + 1/2)], \\ \Delta_j &= V_1 \cos(2\pi\beta j + ih), \end{aligned} \quad (6)$$

with V_1 and V_2 being the modulation amplitudes of the potential and hopping terms, respectively, h being the complex phase, and β being an irrational number to ensure the incommensurate modulation. Hereafter, we choose $\beta = (\sqrt{5} - 1)/2$ as the golden ratio and the lattice site number L from the Fibonacci sequence, and set $t = 1$ as the unit of energy.

The GAA model has rich localization phase diagrams in the Hermitian [98–100] and non-Hermitian cases [6]. By changing the modulation amplitudes V_1 and V_2 (or g), the localization transition of eigenstates between extended, localized, and critical phases can occurs. A typical quantity to characterize localization properties of the

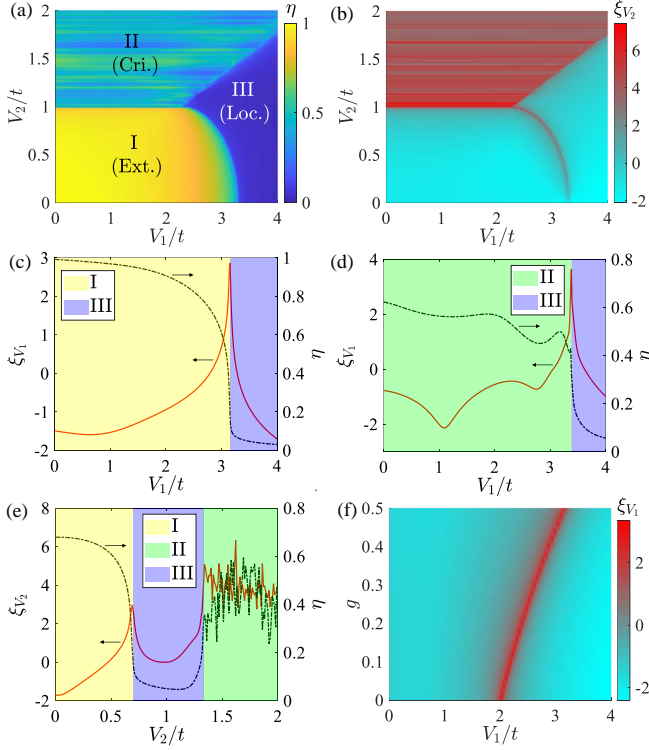


FIG. 1. (Color online) The non-Hermitian GAA model with nonreciprocal hopping given by $H_{\text{GAA}}^{(1)}$ with $L = 610$ under the PBC. (a) η and (b) ξ_{V_2} for the ground state in the parameter space (V_1, V_2) . The localization phase diagram in (a) consists of three regions I, II, III for the extended, critical, and localized phases, respectively. (c,d) ξ_{V_1} and η as a function of V_1 with fixed $V_2 = 0.5$ and $V_2 = 1.5$, respectively. (e) ξ_{V_2} and η as a function of V_2 with fixed $V_1 = 3$. (f) ξ_{V_1} as functions of V_1 and g with fixed $V_2 = 0.5$. The colored phase regions with boundaries in (c-e) are determined by Eq. (8). The non-reciprocal strength is $g = 0.5$ in (a-e). Other parameters are $h = 0$ and $t = 1$.

n -th eigenstate in this model is the fractal dimension:

$$\eta_n = -\frac{\ln(\sum_j^L |\langle j | \psi_n \rangle|^2)}{\ln L}, \quad (7)$$

where $|j\rangle$ is the computational basis and $|\psi_n\rangle$ is the n -th right eigenstates. In this model, there is no mobility edge and all eigenstates share the same localization properties [6, 98–100]. Thus, we focus on the ground state $|\psi_1\rangle$ with the corresponding fractal dimension $\eta_1 \equiv \eta$ for simplicity. When the system size $L \rightarrow \infty$, one has $\eta \rightarrow 1$ for the extended phase, $\eta \rightarrow 0$ for the localized phase, while η falls between 0 and 1 ($\eta \approx 0.5$) in the critical phase, respectively. Figure 1(a) show the numerical results of η in the parameter space (V_1, V_2) for nonreciprocal case with $g = 0.5$ and $h = 0$ under the periodic boundary condition (PBC), by using the exact diagonalization method. Three regimes (denoted by the I, II and III) for the extended, critical, and localized phases are exhibited. Notably, the critical values V_{1c} for localization transition

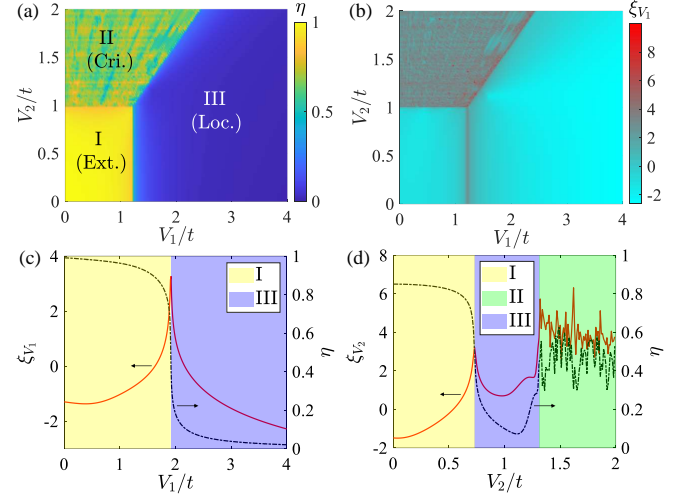


FIG. 2. (Color online) The non-Hermitian GAA model with complex potential phase (and nonreciprocal hopping) given by $H_{\text{GAA}}^{(1)}$ with $L = 610$ under the PBC. (a) η and (b) ξ_{V_1} in the parameter space (V_1, V_2) for $g = 0$. The three regions I, II, and III denotes the extended, critical, and localized phases, respectively. (c) ξ_{V_1} and η as a function of V_1 with fixed $V_2 = 0.5$ and $g = 0.5$. (d) ξ_{V_2} and η as a function of V_2 with fixed $V_1 = 1.8$ and $g = 0.5$. The colored phase regions with boundaries in (c,d) are determined by Eq. (8). Other parameters are $h = 0.5$ and $t = 1$.

points with respect to other parameters are given by [6]

$$V_{1c} = e^{-|h|} \left(2K \cosh |g| + 2\sqrt{K^2 - V_2^2} \sinh |g| \right), \quad (8)$$

with $K = \max(t, V_2)$.

To demonstrate the ability of the non-Hermitian quantum metric to detect localization transition points in non-Hermitian cases, we numerically calculate the diagonal elements of the quantum metric $g_{\mu\mu}$ for the parameter $\mu = \{V_1, V_2\}$. To resolve the three different localization regions in this model, we use the logarithm quantity of the quantum metric

$$\xi_\mu = \log_{10} g_{\mu\mu}, \quad (9)$$

with respect to the model parameters (V_1, V_2, g, h) . We first consider the generalized AA model with only non-reciprocal hopping for fixed $h = 0$ and $g = 0.5$. The numerical result of ξ_{V_2} in Fig. 1(b) shows the boundaries between different localization phase regions, which is consistent with those in Fig. 1(a). To reveal the localization transition points more clearly, we plot ξ_{V_1} and η as a function of V_1 for $V_2 = 0.5$ and $V_2 = 1.5$ in Fig. 1(c) and Fig. 1(d), respectively. The results show that ξ_{V_1} changes relatively smoothly in each phase, while increases significantly and reaches its maximum value at the localization transition points. In Fig. 1(e), we plot ξ_{V_2} and η as a function of V_2 for $V_1 = 3$, which across three localization phases. In this case, we can see that the boundaries between different phases can also be revealed, although

the rapid oscillation of ξ_{V_2} in the critical phase region is exhibited due to the accidental degeneracies of wave functions with respect to V_2 in the critical phase. The quantum metric can even be used to identify the localization transition driven by the non-Hermitian strength g , as shown in Fig. 1(f).

We also consider the GAA model with the complex potential phase for $h = 0.5$ and $g = 0$, with numerical results of η and ξ_{V_1} shown in Fig. 2(a) and Fig. 2(b), respectively. It is evident that the boundaries between the three localization phases distinguished by η corresponds to the peak of ξ_{V_1} . For the case of coexistence of the nonreciprocal hopping and complex potential phase with $g = h = 0.5$, one can still find the peaks of the quantum metric (ξ_{V_1} and ξ_{V_2}) at the localization transition points in Fig. 2(c) and Fig. 2(d). Moreover, we plot three phase regions with different colors in Figs. 1(c-e) and Figs. 2(c,d) according to Eq. (8). One can see that localization transition points in this non-Hermitian GAA model revealed by the quantum metric are perfectly consistent with those obtained from the fractal dimension and the analytical result [6].

B. Revealing mobility edges

We proceed to consider localization transitions of all eigenstates to reveal the mobility edge in non-Hermitian systems with the quantum metric. To do this, we study another non-Hermitian version of the GAA model [3–5]:

$$H_{\text{GAA}}^{(2)} = \sum_j [t(e^{-g}c_{j+1}^\dagger c_j + e^g c_j^\dagger c_{j+1}) + \epsilon_j c_j^\dagger c_j], \quad (10)$$

with a quasi-periodic onsite potential

$$\epsilon_j = \frac{\Delta \cos(2\pi j\beta)}{1 - \alpha \cos(2\pi j\beta)}. \quad (11)$$

Here g represents the nonreciprocal strength of the hopping amplitude, Δ is the amplitude of irrational modulation with $\beta = (\sqrt{5} - 1)/2$, and $\alpha \in (-1, 1)$ denotes the lattice parameter. In the Hermitian case ($g = 0$), when $\alpha = 0$, it reduces to the standard AA model without mobility edges. When $\alpha \neq 0$, this GAA model in the Hermitian limit has an exact mobility edge at energy $E = E_c$ that follows the relationship [3]

$$E_c = \frac{2t - \Delta}{\alpha}. \quad (12)$$

The presence of the mobility edge can be understood by the energy-independent localization transition and self-duality condition driven by the cosine dispersion [3]. This GAA model has been realized with ultracold atoms in tunable synthetic lattices and the mobility edge has been observed [4, 5]. However, the mobility edge in the non-Hermitian GAA model is yet to be explored.

To characterize the localization properties of all eigenstates and reveal the mobility edge in the Hermitian and

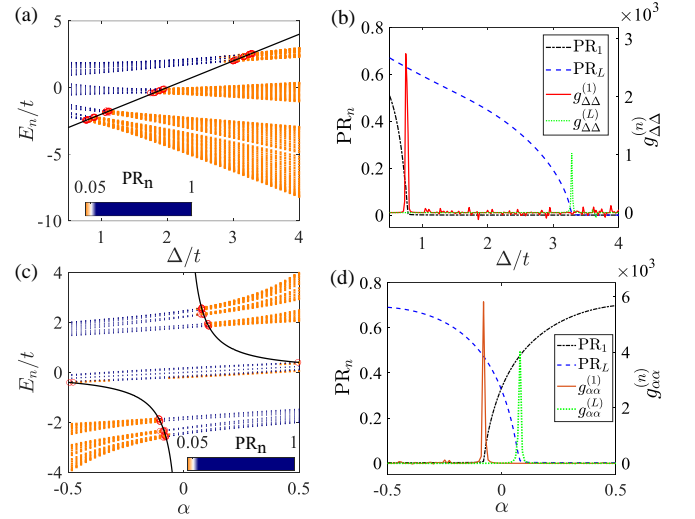


FIG. 3. (Color online) The GAA model given by $H_{\text{GAA}}^{(2)}$ in the Hermitian limit with $L = 610$ under the PBC. The eigenenergies E_n as functions of (a) Δ and (c) α , respectively. The colors correspond to the values of PR_n as the inset color bar. The red circles denote the positions of the peaks of the quantum metric for eigenstates at different Δ or α . The black solid line denotes the exact mobility edge given by Eq. (12). Note that $\text{PR}_n = 0.05$ is set as the critical value for the comparison with the exact mobility edge. (b) PR_n and $g_{\Delta\Delta}^{(n)}$ as functions of Δ for the ground state ($n = 1$) and the highest excited state ($n = L$) with fixed $\alpha = -0.5$. (d) PR_n and $g_{\alpha\alpha}^{(n)}$ as functions of α for the ground state and the highest excited state with fixed $\Delta = 1.8$. Other parameters are $g = 0$ and $t = 1$.

non-Hermitian cases, we can numerically compute the participation ratio of the n -th eigenstate $|\psi_n\rangle$:

$$\text{PR}_n = \frac{1}{L} \frac{1}{\sum_j |\langle j | \psi_n \rangle|^2}. \quad (13)$$

The extended and localized eigenstates take $\text{PR}_n \rightarrow 1$ and $\text{PR}_n \rightarrow 0$, respectively. To detect the mobility edge with the quantum metric, we numerically calculate the corresponding diagonal element of the quantum metric $g_{\mu\mu}^{(n)}$ with $\mu = \{\Delta, \alpha\}$ for the n -th eigenstate $|\psi_n\rangle$.

We first show the numerical results in the Hermitian limit with $g = 0$ in Fig. 3. As shown in Fig. 3(a), the mobility edge exhibits and separates the eigenstates from PR_n : the upper ones as extended states while the lower ones are localized states. The peak positions of $g_{\Delta\Delta}^{(n)}$ and the exact mobility edge given by Eq. (12) are plotted, which are consistent with each other. To be more clearly, we show $g_{\Delta\Delta}^{(n)}$ and PR_n as a function of Δ for the ground state ($n = 1$) and the highest excited state ($n = L$) in Fig. 3(b), where $g_{\Delta\Delta}^{(n)}$ exhibits a distinct peak at the critical point with $\text{PR}_n \approx 0$. The mobility edge separating extended and localized eigenstates with respect to varying the parameter α can be also revealed by the quantum metric $g_{\alpha\alpha}^{(n)}$, as shown in Figs. 3(c,d).

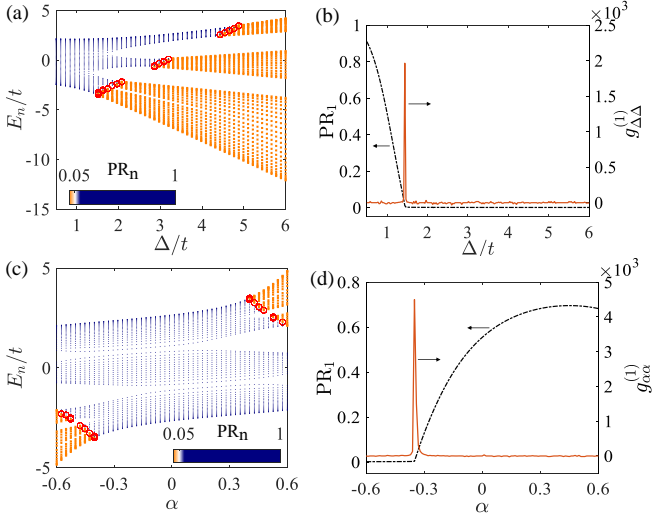


FIG. 4. (Color online) The non-Hermitian GAA model given by $H_{\text{GAA}}^{(2)}$ with $L = 610$ under the PBC. The eigenenergies E_n as functions of (a) Δ and (c) α , respectively. The red circles denote the positions of the peaks of the quantum metric for eigenstates at different Δ or α . (b) PR_1 and $g_{\Delta\Delta}^{(1)}$ as a function of Δ for the ground state with fixed $\alpha = -0.5$. (d) PR_1 and $g_{\alpha\alpha}^{(1)}$ as a function of α for the ground state with fixed $\Delta = 1.8$. Other parameters are $g = 0.5$ and $t = 1$.

For the non-Hermitian case, the nonreciprocal strength g modify the mobility edge from the exact form, with two examples of $g = 0.5$ shown in Fig. 4. In these cases, the localization transitions of right eigenstates with respect to the parameters Δ (α) are revealed by $g_{\Delta\Delta}^{(n)}$ ($g_{\alpha\alpha}^{(n)}$) in Fig. 4(a) [4(c)]. Figure 4(b) [4(d)] shows PR_1 and $g_{\Delta\Delta}^{(1)}$ ($g_{\alpha\alpha}^{(1)}$) as a function of Δ (α) for the ground state. One can find the peak of $g_{\Delta\Delta}^{(1)}$ ($g_{\alpha\alpha}^{(1)}$) is exhibited at the localization transition point. Comparing with the Hermitian case, the mobility edge with respect to Δ moves to the larger values of Δ in Fig 4(a), while it moves towards larger $|\alpha|$ in Figs 4(c). This can be understood by the delocalization enhanced by the nonreciprocal hopping [9, 63, 64]. Thus, our results demonstrate the quantum metric can be used to reveal the mobility edge in both the Hermitian and non-Hermitian systems.

IV. QUANTUM PHASE TRANSITIONS IN NON-HERMITIAN MANY-BODY SYSTEMS

A. Non-Hermitian cluster Ising model

We proceed to reveal the quantum phase transition of many-body ground states in non-Hermitian interacting spin systems with the quantum metric. We first consider the non-Hermitian cluster Ising model with exactly solvable ground states [101], which takes the following

Hamiltonian

$$H_{\text{NH-Ising}}^{(1)} = -J \sum_{l=1}^N \sigma_{l-1}^x \sigma_l^z \sigma_{l+1}^x + \lambda \sum_{l=1}^N \sigma_l^y \sigma_{l+1}^y + \frac{i\Gamma}{2} \sum_{l=1}^N \sigma_l^u, \quad (14)$$

where $\sigma_l^{x,y,z}$ denote the Pauli matrices of the l -th spin, and the gain and loss is given by $\sigma_l^u = \begin{pmatrix} 1 & 0 \\ 0 & 0 \end{pmatrix}$. There are three parameters in this model: J represents the cluster exchange strength, λ denotes the Ising exchange strength, and Γ signifies the strength of gain or loss. In the rest of this section, we set $J = 1$ as the energy unit.

Using the standard Jordan-Wigner transformation and the Fourier transformation under the PBC, we can obtain the Hamiltonian in momentum space, which is given by

$$H_k = 2 \sum_{k>0} [iy_k (c_k^\dagger c_{-k}^\dagger + c_k c_{-k}) + z_k (c_k^\dagger c_k + c_{-k}^\dagger c_{-k} - 1)], \quad (15)$$

here $y_k = \sin(2k) + \lambda \sin(k)$ and $z_k = \cos(2k) - \lambda \cos(k) - \frac{i\Gamma}{4}$. By diagonalizing H_k through the Bogoliubov transformation, one can obtain the ground state of this model

$$|G\rangle = \prod_{k>0} [\cos(\frac{\theta_k}{2}) + i \sin(\frac{\theta_k}{2}) c_k^\dagger c_{-k}^\dagger] |\text{Vac}\rangle, \quad (16)$$

where $|\text{Vac}\rangle$ is the vacuum state of the free fermion and $\theta_k = \arctan(-y_k/z_k)$. The properties of the ground state can be characterized by the staggered magnetization m_y and the string order parameter O^x . The staggered magnetization m_y is determined by the spin-correlation function R_r^y with the following relationship

$$m_y^2 = \lim_{r \rightarrow \infty} (-1)^r R_r^y = \lim_{r \rightarrow \infty} (-1)^r \langle G | \sigma_{l+r}^y \sigma_l^y | G \rangle, \quad (17)$$

where r is the relative distance between spins and l ($l \in [1, N]$) is an irrelevant index under the PBC. Using the Wick theorem [102], R_r^y can be transformed to a Toeplitz determinant

$$R_r^y = \begin{vmatrix} D_1 & D_0 & \cdots & D_{-r+2} \\ D_2 & D_1 & \cdots & D_{-r+3} \\ \vdots & \vdots & \ddots & \vdots \\ D_r & D_{r-1} & \cdots & D_1 \end{vmatrix}, \quad (18)$$

with the elements

$$D_r = \frac{1}{\pi} \int_0^\pi dk \frac{\cos[(r+2)k] - \lambda \cos[(r-1)k]}{\sqrt{1 + \lambda^2 - 2\lambda \cos(3k)}}. \quad (19)$$

The second order parameter is the string order parameter O^x , which is given by

$$O^x = \lim_{r \rightarrow \infty} (-1)^r \langle G | \sigma_1^x \sigma_2^y \left(\prod_{l=3}^r \sigma_l^z \right) \sigma_{r+1}^y \sigma_{r+2}^x | G \rangle. \quad (20)$$

Using the same method in Ref. [102], one can rewrite O^x

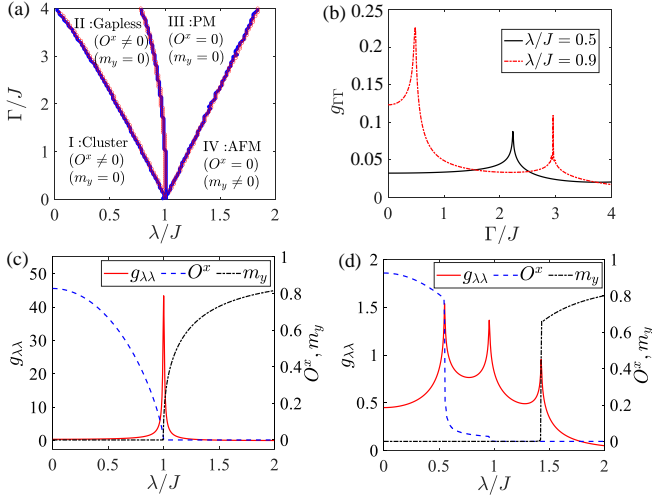


FIG. 5. (Color online) The non-Hermitian cluster Ising model $H_{\text{NH-Ising}}^{(1)}$ under the PBC. (a) The phase diagram with boundaries (blue solid lines) determined by the order parameters O^x and m_y . Four regions I, II, III, IV denote the cluster, gapless, paramagnetic, and antiferromagnetic phases, respectively. The locations of the peaks of the quantum metric are plotted as the red circles and consistent with the phase boundaries. (b) $g_{\Gamma\Gamma}$ as a function of Γ with fixed $\lambda = 0.5$ and $\lambda = 0.9$. (c) In the Hermitian limit with $\Gamma = 0$ and (d) in the non-Hermitian case with $\Gamma = 2$, $g_{\lambda\lambda}$, O^x , and m_y as a function of λ . Other parameter is $J = 1$.

as

$$O^x = \lim_{r \rightarrow \infty} \begin{vmatrix} G_{-2} & G_{-3} & \dots & G_{-r-1} \\ G_{-1} & G_{-2} & \dots & G_{-r} \\ G_0 & G_{-1} & \dots & G_{-r+1} \\ \vdots & \vdots & \ddots & \vdots \\ G_{r-2} & G_{r-5} & \dots & G_{-3} \\ G_{r-3} & G_{r-4} & \dots & G_{-2} \end{vmatrix}, \quad (21)$$

where $G_r = \frac{1}{\pi} \int_0^\pi dk [\cos(kr) \cos(\theta_k) + \sin(kr) \sin(\theta_k)]$.

By numerically calculating the order parameters O^x and m_y for $r = 1000$ that is large enough to approach the thermodynamic limit, one can obtain four phases in the phase diagram in the λ - Γ plane [101], as shown in Fig. 5(a). The first one is the gapped cluster phase with long-range correlation ($O^x \neq 0$) and vanishing staggered magnetization ($m_y = 0$). The second one is the gapless phase with the power-law decay of correlation ($O^x \neq 0$ for finite systems) and vanishing staggered magnetization ($m_y = 0$). The third and fourth ones are the conventional paramagnetic ($m_y = 0$) and antiferromagnetic ($m_y \neq 0$) without long-range correlation, respectively. The phase boundaries determined by the order parameters are plotted as the blue solid lines in Fig. 5(a). To show that the quantum phase transition points in this non-Hermitian cluster Ising model can be revealed by the quantum metric, we plot the locations of the peaks of $g_{\mu\mu}$ of the ground state $|G\rangle$ for the parameter $\mu = \{\lambda, \Gamma\}$. As shown in Fig. 5(a), the locations of the peaks correspond

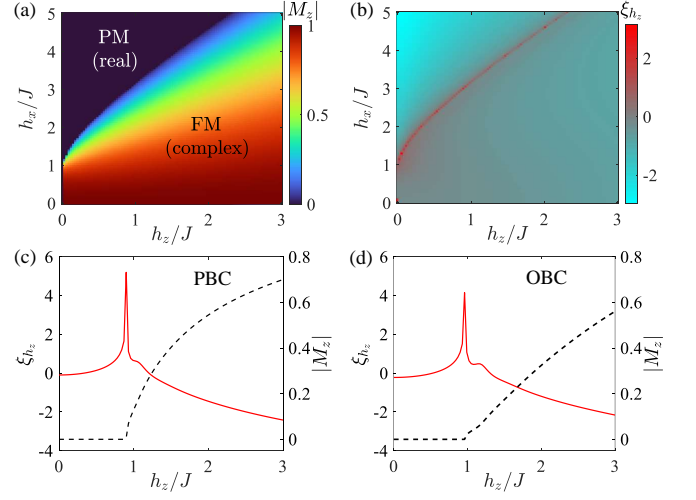


FIG. 6. (Color online) The non-Hermitian mixed-field Ising model $H_{\text{NH-Ising}}^{(2)}$ with the system size $N = 10$. (a) $|M_z|$ and (b) ξ_{h_z} of the ground state as functions of h_z and h_x under periodic boundary condition. The phase diagram based on $|M_z|$ consists two regions I and II for the paramagnetic and ferromagnetic phases with real and complex energies, respectively. $|M_z|$ and ξ_{h_z} as a function of h_z (c) under the PBC; and (d) the OBC, respectively. Other parameter is $J = 1$.

to the critical points of the four different phases. To illustrate more clearly, we plot $g_{\Gamma\Gamma}$ as a function of Γ in Fig. 5(b). One can still find the peaks at $\Gamma \approx 2.23$ with fixed $\lambda = 0.5$, and at $\Gamma \approx 0.48$ and $\Gamma \approx 2.95$ with fixed $\lambda = 0.9$ in $g_{\Gamma\Gamma}$, indicating one and two quantum critical points, respectively. We further plot $g_{\lambda\lambda}$ as a function of λ in the Hermitian ($\Gamma = 0$) and non-Hermitian case ($\Gamma = 2$) in Fig. 5(c) and Fig. 5(d), respectively. The results show that the values of $g_{\lambda\lambda}$ exhibit peaks at the quantum phase transition points where the behaviours of the order parameters O^x and m_y change.

B. Non-Hermitian mixed-field Ising model

We further study the non-Hermitian mixed-field Ising model, which is non-integrable and described by the following Hamiltonian

$$H_{\text{NH-Ising}}^{(2)} = -J \sum_{l=1}^N \sigma_l^z \sigma_{l+1}^z + h_x \sum_{l=1}^N \sigma_l^x + i h_z \sum_{l=1}^N \sigma_l^z, \quad (22)$$

where h_x and h_z denote the strengths of the real and imaginary fields that are along the transverse and longitudinal directions, respectively. The order parameter for the ground state $|\psi_1\rangle$ in this model is the magnetization $M_z = \frac{1}{N} \langle \psi_1 | \sum_{l=1}^N \sigma_l^z | \psi_1 \rangle$, where $|\psi_1\rangle$ can be numerically obtained by the exact diagonalization method for small system size N . The numerical results for $N = 10$ under the PBC and the open boundary condition (OBC) are shown in Figs. 6(a-c) and Fig. 6(d), respectively.

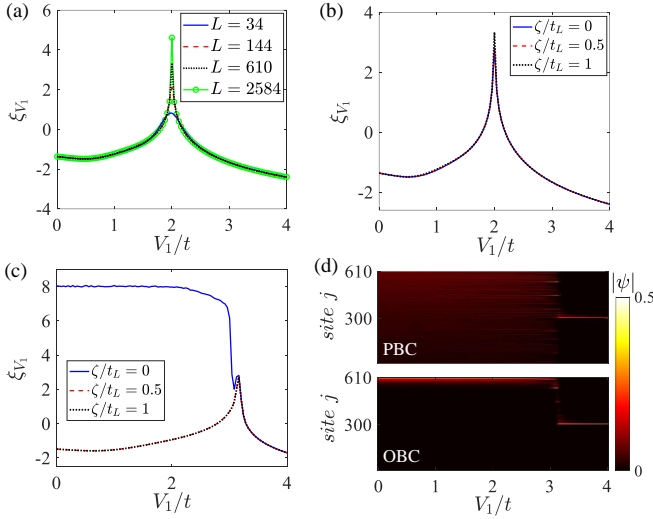


FIG. 7. (Color online) (a) ξ_{V_1} as a function of V_1 for $H_{\text{GAA}}^{(1)}$ with different system sizes L and fixed $g = h = 0$ under periodic boundary condition. ξ_{V_1} as a function of V_1 for \tilde{H} [see Eq. (23)] with fixed (b) $g = 0$; and (c) $g = 0.5$, for different boundary condition coefficients ζ . (d) The probability amplitudes of the ground-state wave functions as a function of V_1 under the PBC and the OBC, respectively. The system size in (b-d) is $L = 610$. Other parameters are $h = 0$, $V_2 = 0.5$, and $t = 1$.

The phase diagram that contains the paramagnetic phase with $|M_z| \approx 0$ (and real energy) and the ferromagnetic phase with finite value of $|M_z|$ (and complex energy) in the h_z - h_x parameter plane is shown in Fig. 6(a). Moreover, the phase transition between two phases is accompanied by a real-complex transition of the ground state energy. To detect the phase transition with the quantum metric, we numerically compute the logarithm quantify of quantum metric $\xi_{h_z} = \log_{10} g_{h_z h_z}$ as a function of h_z and h_x in Fig 6(b). One can see the boundary between the paramagnetic and ferromagnetic phases are well revealed by ξ_{h_z} . As shown in Fig. 6(c) and Fig. 6(d) for different boundary conditions with fixed $h_x = 3$, the critical point $h_z \approx 0.9$ and $h_z \approx 0.96$ can both be clearly revealed by the quantum metric.

V. DISCUSSION AND CONCLUSION

Before concluding, we discuss the finite-size effect and boundary conditions on detecting the non-Hermitian critical points with the quantum metric. Without loss of generality, we focus on the non-Hermitian GAA model $H_{\text{GAA}}^{(1)}$ in Eq. (5). The finite-size scaling of the quantum metric of the ground state $\xi_{V_1} = \log_{10} g_{V_1 V_1}$ under the PBC for the lattice sizes $L = 34, 144, 610, 2584$ (chosen from the Fibonacci sequences) is shown in Fig 7(a). One can find that the critical point can be revealed by the peak of the quantum metric even for a small lattice of $L = 34$, and the peak becomes higher as the lattice

size is increased. To consider the boundary effect on the quantum metric, we add an boundary coupling term to the Hamiltonian $H_{\text{GAA}}^{(1)}$ as

$$\tilde{H} = H_{\text{GAA}}^{(1)} + \xi(e^{-g}c_1^\dagger c_L + e^g c_L^\dagger c_1), \quad (23)$$

where ζ is the coefficient for tuning different boundary conditions. For $\zeta = 0$, it denotes the open boundary condition, while $\zeta = 1$ ($\zeta \neq 0, 1$) denotes the standard (modified) periodic boundary condition. As shown in Fig. 7(b), the results of ξ_{V_1} as a function of V_1 under different boundary conditions ($\zeta = 0, 0.5, 1$) coincide in the Hermitian limit. In the non-Hermitian case, the results of ξ_{V_1} are different for periodic ($\zeta = 0.5, 1$) and open ($\zeta = 0$) boundary conditions, while the transition point can be revealed in both conditions, as shown in Fig 7(c). The difference comes from the localized bulk eigenstates induced by the non-Hermitian skin effect under the open boundary condition [75, 77], as shown in Fig 7(d). The non-Hermitian skin effect destroys the extended phase under the original periodic boundary condition and leads to the increase of the quantum metric with accidental degeneracies. Thus, our results are robust against the finite-size effect and different boundary conditions when using the quantum metric to reveal critical points.

In summary, we have investigated the quantum phase transitions in various non-Hermitian systems by using the information-geometric approach. It has been shown that the peaks of the quantum metric of the eigenstates exactly identify the localization transition points and mobility edges in the non-Hermitian GAA models. For non-Hermitian cluster and mixed-field Ising models, we have demonstrated that the phase boundaries in the non-Hermiticity parameter space determined by quantum metric of ground state perfectly coincide with those from the corresponding order parameters. These results indicate that the peak of the quantum metric serving as good signatures for detecting the non-Hermitian critical points in both single-particle and many-body systems. This strategy is robust against the finite-size effect and different boundary conditions. Notably, our present work only focuses on the right eigenstates of non-Hermitian Hamiltonians, and the quantum metric effect based on the biorthogonal eigenstates and the non-unitary dynamics are deserving to be further explored.

-Note added. After finishing our manuscript, we noticed two relevant preprints [103, 104]. In Ref. [103], a generalization of the QGT based on the generator of adiabatic transformations was developed to study phase transitions in non-Hermitian quantum systems. In Ref. [104], the self-normal and biorthogonal fidelity susceptibilities were used to study the critical behaviors in the nonreciprocal Aubry-André-Harper model.

ACKNOWLEDGMENTS

We thank Zhi Li for helpful discussions. This work was supported by the National Natural Science Founda-

tion of China (Grant No. 12174126), the Guangdong Basic and Applied Basic Research Foundation (Grant No.

2024B1515020018), and the Science and Technology Program of Guangzhou (Grant No. 2024A04J3004).

-
- [1] S. Sachdev, *Quantum Phase Transitions*, 2nd ed. (Cambridge University Press, 2011).
 - [2] P. Smacchia, L. Amico, P. Facchi, R. Fazio, G. Florio, S. Pascazio, and V. Vedral, *Phys. Rev. A* **84**, 022304 (2011).
 - [3] S. Ganesan, J. H. Pixley, and S. Das Sarma, *Phys. Rev. Lett.* **114**, 146601 (2015).
 - [4] F. A. An, K. Padavić, E. J. Meier, S. Hegde, S. Ganesan, J. H. Pixley, S. Vishveshwara, and B. Gadway, *Phys. Rev. Lett.* **126**, 040603 (2021).
 - [5] Y. Wang, J.-H. Zhang, Y. Li, J. Wu, W. Liu, F. Mei, Y. Hu, L. Xiao, J. Ma, C. Chin, and S. Jia, *Phys. Rev. Lett.* **129**, 103401 (2022).
 - [6] L.-Z. Tang, G.-Q. Zhang, L.-F. Zhang, and D.-W. Zhang, *Phys. Rev. A* **103**, 033325 (2021).
 - [7] N. Matsumoto, K. Kawabata, Y. Ashida, S. Furukawa, and M. Ueda, *Phys. Rev. Lett.* **125**, 260601 (2020).
 - [8] S. Longhi, *Phys. Rev. Lett.* **122**, 237601 (2019).
 - [9] Z. Gong, Y. Ashida, K. Kawabata, K. Takasan, S. Higashikawa, and M. Ueda, *Phys. Rev. X* **8**, 031079 (2018).
 - [10] G.-Q. Zhang, L.-Z. Tang, L.-F. Zhang, D.-W. Zhang, and S.-L. Zhu, *Phys. Rev. B* **104**, L161118 (2021).
 - [11] P. Zanardi and N. Paunković, *Phys. Rev. E* **74**, 031123 (2006).
 - [12] S.-L. Zhu, *Phys. Rev. Lett.* **96**, 077206 (2006).
 - [13] S.-L. Zhu, *Int. J. Mod. Phys. B* **22**, 561 (2008).
 - [14] P. Zanardi, P. Giorda, and M. Cozzini, *Phys. Rev. Lett.* **99**, 100603 (2007).
 - [15] W.-L. You, Y.-W. Li, and S.-J. Gu, *Phys. Rev. E* **76**, 022101 (2007).
 - [16] S.-J. Gu, *Int. J. Mod. Phys. B* **24**, 4371 (2010).
 - [17] Y.-Q. Ma, S. Chen, H. Fan, and W.-M. Liu, *Phys. Rev. B* **81**, 245129 (2010).
 - [18] A. Carollo, D. Valenti, and B. Spagnolo, *Phys. Rep.* **838**, 1 (2020).
 - [19] M. Kolodrubetz, D. Sels, P. Mehta, and A. Polkovnikov, *Phys. Rep.* **697**, 1 (2017).
 - [20] H.-T. Ding, C.-X. Zhang, J.-X. Liu, J.-T. Wang, D.-W. Zhang, and S.-L. Zhu, *Phys. Rev. A* **109**, 043305 (2024).
 - [21] H.-T. Ding, Y.-Q. Zhu, P. He, Y.-G. Liu, J.-T. Wang, D.-W. Zhang, and S.-L. Zhu, *Phys. Rev. A* **105**, 012210 (2022).
 - [22] P. Törmä, *Phys. Rev. Lett.* **131**, 240001 (2023).
 - [23] J. Provost and G. Vallee, *Commun. Math. Phys.* **76**, 289 (1980).
 - [24] D. J. Thouless, M. Kohmoto, M. P. Nightingale, and M. den Nijs, *Phys. Rev. Lett.* **49**, 405 (1982).
 - [25] B. Simon, *Phys. Rev. Lett.* **51**, 2167 (1983).
 - [26] M. Berry, *Proc. R. Soc. Lond. A* **392**, 45 (1984).
 - [27] W. Guo, W. Zhong, X.-X. Jing, L.-B. Fu, and X. Wang, *Phys. Rev. A* **93**, 042115 (2016).
 - [28] G. Sundaram and Q. Niu, *Phys. Rev. B* **59**, 14915 (1999).
 - [29] N. Nagaosa, J. Sinova, S. Onoda, A. H. MacDonald, and N. P. Ong, *Rev. Mod. Phys.* **82**, 1539 (2010).
 - [30] Y. Aharonov and D. Bohm, *Phys. Rev.* **115**, 485 (1959).
 - [31] M. Z. Hasan and C. L. Kane, *Rev. Mod. Phys.* **82**, 3045 (2010).
 - [32] X.-L. Qi and S.-C. Zhang, *Rev. Mod. Phys.* **83**, 1057 (2011).
 - [33] D.-W. Zhang, Y.-Q. Zhu, Y. Zhao, H. Yan, and S.-L. Zhu, *Adv. Phys.* **67**, 253 (2018).
 - [34] A. Julku, S. Peotta, T. I. Vanhala, D.-H. Kim, and P. Törmä, *Phys. Rev. Lett.* **117**, 045303 (2016).
 - [35] P. He, H.-T. Ding, and S.-L. Zhu, *Phys. Rev. A* **103**, 043329 (2021).
 - [36] R. Roy, *Phys. Rev. B* **90**, 165139 (2014).
 - [37] L.-K. Lim, J.-N. Fuchs, and G. Montambaux, *Phys. Rev. A* **92**, 063627 (2015).
 - [38] G. Palumbo and N. Goldman, *Phys. Rev. Lett.* **121**, 170401 (2018).
 - [39] X. Tan, D.-W. Zhang, Z. Yang, J. Chu, Y.-Q. Zhu, D. Li, X. Yang, S. Song, Z. Han, Z. Li, Y. Dong, H.-F. Yu, H. Yan, S.-L. Zhu, and Y. Yu, *Phys. Rev. Lett.* **122**, 210401 (2019).
 - [40] X. Tan, D.-W. Zhang, W. Zheng, X. Yang, S. Song, Z. Han, Y. Dong, Z. Wang, D. Lan, H. Yan, S.-L. Zhu, and Y. Yu, *Phys. Rev. Lett.* **126**, 017702 (2021).
 - [41] Q. Liao, C. Leblanc, J. Ren, F. Li, Y. Li, D. Solnyshkov, G. Malpuech, J. Yao, and H. Fu, *Phys. Rev. Lett.* **127**, 107402 (2021).
 - [42] M. Chen, C. Li, G. Palumbo, Y.-Q. Zhu, N. Goldman, and P. Cappellaro, *Science* **375**, 1017 (2022).
 - [43] L. Asteria, D. T. Tran, T. Ozawa, M. Tarnowski, B. S. Rem, N. Fläschner, K. Sengstock, N. Goldman, and C. Weitenberg, *Nat. Phys.* **15**, 449 (2019).
 - [44] M. Yu, Y. Liu, P. Yang, M. Gong, Q. Cao, S. Zhang, H. Liu, M. Heyl, T. Ozawa, N. Goldman, et al., *npj Quantum Information* **8**, 56 (2022).
 - [45] W. Zheng, J. Xu, Z. Ma, Y. Li, Y. Dong, Y. Zhang, X. Wang, G. Sun, P. Wu, J. Zhao, S. Li, D. Lan, X. Tan, and Y. Yu, *Chin. Phys. Lett.* **39**, 100202 (2022).
 - [46] M. Lysne, M. Schüler, and P. Werner, *Phys. Rev. Lett.* **131**, 156901 (2023).
 - [47] X. Tan, D.-W. Zhang, Q. Liu, G. Xue, H.-F. Yu, Y.-Q. Zhu, H. Yan, S.-L. Zhu, and Y. Yu, *Phys. Rev. Lett.* **120**, 130503 (2018).
 - [48] M. Yu, P. Yang, M. Gong, Q. Cao, Q. Lu, H. Liu, S. Zhang, M. B. Plenio, F. Jelezko, T. Ozawa, N. Goldman, and J. Cai, *Natl. Sci. Rev.* **7**, 254 (2019).
 - [49] M. Yu, X. Li, Y. Chu, B. Mera, F. N. Ünal, P. Yang, Y. Liu, N. Goldman, and J. Cai, *Natl. Sci. Rev.*, nwae065 (2024).
 - [50] A. Gianfrate, O. Bleu, L. Dominici, V. Ardizzone, M. De Giorgi, D. Ballarini, G. Lerario, K. West, L. Pfeiffer, D. Solnyshkov, et al., *Nature* **578**, 381 (2020).
 - [51] C.-R. Yi, J. Yu, H. Yuan, R.-H. Jiao, Y.-M. Yang, X. Jiang, J.-Y. Zhang, S. Chen, and J.-W. Pan, *Phys. Rev. Res.* **5**, L032016 (2023).
 - [52] J. Cuerda, J. M. Taskinen, N. Källman, L. Grabitz, and P. Törmä, *arXiv:2305.13174*.
 - [53] D. D. Solnyshkov, C. Leblanc, L. Bessonart, A. Nalitov,

- J. Ren, Q. Liao, F. Li, and G. Malpuech, *Phys. Rev. B* **103**, 125302 (2021).
- [54] L. Campos Venuti and P. Zanardi, *Phys. Rev. Lett.* **99**, 095701 (2007).
- [55] P. Zanardi, P. Giorda, and M. Cozzini, *Phys. Rev. Lett.* **99**, 100603 (2007).
- [56] H.-L. Zhang, J.-H. Lv, K. Chen, X.-J. Yu, F. Wu, Z.-B. Yang, and S.-B. Zheng, [arXiv:2312.14414](#).
- [57] D. F. Abasto, A. Hamma, and P. Zanardi, *Phys. Rev. A* **78**, 010301 (2008).
- [58] B. Hetényi and P. Lévy, *Phys. Rev. A* **108**, 032218 (2023).
- [59] A. F. Albuquerque, F. Alet, C. Sire, and S. Capponi, *Phys. Rev. B* **81**, 064418 (2010).
- [60] A. Dey, S. Mahapatra, P. Roy, and T. Sarkar, *Phys. Rev. E* **86**, 031137 (2012).
- [61] H.-L. Zhang, J.-H. Lv, K. Chen, X.-J. Yu, F. Wu, Z.-B. Yang, and S.-B. Zheng, “Critical quantum geometric tensors of parametrically-driven nonlinear resonators,” (2023), [arXiv:2312.14414 \[quant-ph\]](#).
- [62] Y. Ashida, Z. Gong, and M. Ueda, *Advances in Physics* **69**, 249 (2020).
- [63] N. Hatano and D. R. Nelson, *Phys. Rev. Lett.* **77**, 570 (1996).
- [64] N. Hatano and D. R. Nelson, *Phys. Rev. B* **56**, 8651 (1997).
- [65] C. M. Bender and S. Boettcher, *Phys. Rev. Lett.* **80**, 5243 (1998).
- [66] T. Liu, Y.-R. Zhang, Q. Ai, Z. Gong, K. Kawabata, M. Ueda, and F. Nori, *Phys. Rev. Lett.* **122**, 076801 (2019).
- [67] K. Kawabata, S. Higashikawa, Z. Gong, Y. Ashida, and M. Ueda, *Nat. Commun.* **10**, 297 (2019).
- [68] Y. Chen and H. Zhai, *Phys. Rev. B* **98**, 245130 (2018).
- [69] D.-W. Zhang, Y.-L. Chen, G.-Q. Zhang, L.-J. Lang, Z. Li, and S.-L. Zhu, *Phys. Rev. B* **101**, 235150 (2020).
- [70] Y. M. R. Hu, E. A. Ostrovskaya, and E. Estrecho, [arXiv:2306.00351](#).
- [71] Y.-T. Tu, I. Jang, P.-Y. Chang, and Y.-C. Tzeng, *Quantum* **7**, 960 (2023).
- [72] Y.-C. Tzeng, C.-Y. Ju, G.-Y. Chen, and W.-M. Huang, *Phys. Rev. Res.* **3**, 013015 (2021).
- [73] D. Sticlet, C. P. Moca, and B. Dóra, *Phys. Rev. B* **108**, 075133 (2023).
- [74] B. Dóra, D. Sticlet, and C. P. Moca, *Phys. Rev. Lett.* **128**, 146804 (2022).
- [75] S.-Y. Yao and Z. Wang, *Phys. Rev. Lett.* **121**, 086803 (2018).
- [76] H. Jiang, L.-J. Lang, C. Yang, S.-L. Zhu, and S. Chen, *Phys. Rev. B* **100**, 054301 (2019).
- [77] F. Song, S. Yao, and Z. Wang, *Phys. Rev. Lett.* **123**, 246801 (2019).
- [78] L.-Z. Tang, L.-F. Zhang, G.-Q. Zhang, and D.-W. Zhang, *Phys. Rev. A* **101**, 063612 (2020).
- [79] D.-W. Zhang, L.-Z. Tang, L.-J. Lang, H. Yan, and S.-L. Zhu, *Sci. China-Phys. Mech. Astron.* **63**, 267062 (2020).
- [80] H.-F. Liu, Z.-X. Su, Z.-Q. Zhang, and H. Jiang, *Chin. Phys. B* **29**, 050502 (2020).
- [81] L.-J. Zhai, S. Yin, and G.-Y. Huang, *Phys. Rev. B* **102**, 064206 (2020).
- [82] T. Liu, H. Guo, Y. Pu, and S. Longhi, *Phys. Rev. B* **102**, 024205 (2020).
- [83] R. Hamazaki, K. Kawabata, and M. Ueda, *Phys. Rev. Lett.* **123**, 090603 (2019).
- [84] J. Li, H.-T. Ding, and D.-W. Zhang, *Acta Phys. Sin.* **72**, 200601 (2023).
- [85] Q. Liao, C. Leblanc, J. Ren, F. Li, Y. Li, D. Solnyshkov, G. Malpuech, J. Yao, and H. Fu, *Phys. Rev. Lett.* **127**, 107402 (2021).
- [86] E. J. Bergholtz, J. C. Budich, and F. K. Kunst, *Reviews of Modern Physics* **93**, 015005 (2021).
- [87] V. M. Alvarez, J. B. Vargas, and L. F. Torres, *Phys. Rev. B* **97**, 121401 (2018).
- [88] K. D. Agarwal, T. K. Konar, L. G. C. Lakkaraju, and A. S. De, “Detecting exceptional point through dynamics in non-hermitian systems,” (2022), [arXiv:2212.12403 \[quant-ph\]](#).
- [89] K. D. Agarwal, T. K. Konar, L. G. C. Lakkaraju, and A. S. De, “Recognizing critical lines via entanglement in non-hermitian systems,” (2023), [arXiv:2305.08374 \[quant-ph\]](#).
- [90] R. Di Candia, F. Minganti, K. Petrovnin, G. Paraoanu, and S. Felicetti, *npj Quantum Information* **9**, 23 (2023).
- [91] H. Liang, Y. Su, X. Xiao, Y. Che, B. C. Sanders, and X. Wang, *Phys. Rev. A* **102**, 013722 (2020).
- [92] W.-T. He, C.-W. Lu, Y.-X. Yao, H.-Y. Zhu, and Q. Ai, *Front. Phys.* **18**, 31304 (2023).
- [93] P. G. Harper, *Proc. Phys. Soc. Sect. A* **68**, 874 (1955).
- [94] S. Aubry and G. André, *Ann. Israel Phys. Soc.* **3**, 18 (1980).
- [95] S.-Z. Li, X.-J. Yu, and Z. Li, *Physical Review B* **109**, 024306 (2024).
- [96] C.-C. Ye, W. L. Vleeshouwers, S. Heatley, V. Gritsev, and C. M. Smith, [arXiv:2305.17675](#).
- [97] G. Sun, J.-C. Tang, and S.-P. Kou, *Frontiers of Physics* **17**, 1 (2022).
- [98] I. Chang, K. Ikezawa, and M. Kohmoto, *Phys. Rev. B* **55**, 12971 (1997).
- [99] F. Liu, S. Ghosh, and Y. D. Chong, *Phys. Rev. B* **91**, 014108 (2015).
- [100] Y. Wang, C. Cheng, X.-J. Liu, and D. Yu, *Phys. Rev. Lett.* **126**, 080602 (2021).
- [101] Z.-X. Guo, X.-J. Yu, X.-D. Hu, and Z. Li, *Phys. Rev. A* **105**, 053311 (2022).
- [102] G. C. Wick, *Phys. Rev.* **80**, 268 (1950).
- [103] P. Orlov, G. V. Shlyapnikov, and D. V. Kurlov, “Adiabatic transformations in dissipative and non-hermitian phase transitions,” (2024), [arXiv:2404.12337 \[quant-ph\]](#).
- [104] C.-C. Zeng, Z. Cai, G.-H. Wang, and G. Sun, “Fidelity and criticality in the nonreciprocal aubry-andré-harper model,” (2024), [arXiv:2404.16704 \[cond-mat.dis-nn\]](#).